Longitudinal Tension Variation in Collapsible Channels: A New Mechanism for the Breakdown of Steady Flow

T. J. Pedley
Department of Applied Mathematical Studies, University of Leeds, Leeds LS2 9JT, U.K.

There are several mechanisms potentially involved in the breakdown of steady fluid flow in a collapsible tube under external pressure. Here we investigate one that has received little attention in the past: the fact that the longitudinal tension in the tube wall, T, *decreases with distance downstream as a consequence of the viscous shear stress exerted by the fluid. If the tube is long enough, or the initial tension small enough,* T *may fall to zero before the end of the collapsible tube, and unsteady motion would presumably then ensue; this is what we mean by "breakdown." We study the phenomenon theoretically, when the flow Reynolds number is of order one, using lubrication theory in a symmetric two-dimensional channel in which the collapsible tube is replaced by membranes occupying a segment of each wall. The resulting nonlinear ordinary differential equations are solved numerically for values of the dimensionless parameters that cover all the qualitatively different types of solution (e.g., in which the channel is distended over all its length, collapsed over all its length, or distended in the upstream part and collapsed downstream). Reducing the longitudinal tension has a marked effect on the shape of the collapsible segment, causing it to become much more deformed for the same flow rate and external pressure. Indeed, the wall slope is predicted to become very large when the downstream tension is very small, so the model is not self-consistent then. Nevertheless, the parameter values for which* T *becomes zero are mapped out and are expected to be qualitatively useful. The relationships between the values of* T *during flow and its value before the flow begins is also considered.*

1 Introduction

There are numerous physiological examples of elastic tubes through which fluid flows, steadily or unsteadily, with internal pressure below the external pressure so there is a tendency for the tube to collapse. Examples include veins, coronary arteries, large airways, the ureters and urethra, etc, (see [11, 17] for suitable reviews). Many workers (e.g., [2, 3, 5, 7]) have performed laboratory experiments to investigate collapsible tube flow: a segment of collapsible tube is mounted (usually with some longitudinal tension) between two rigid tubes and is contained in a chamber whose pressure P_e can be independently controlled. Fluid is driven at volume flow rate Q through the tube by the maintenance of a steady reservoir pressure Pr far upstream, which exceeds both P_e and the far downstream pressure P_d. In steady flow experiments the pressure drop along the collapsible segment, ΔP, is plotted against Q; different results are obtained depending on what pressure difference is held constant as Q is varied [11].

In virtually all reported experiments, except those at very low Reynolds number, the steady flow gives way to self-excited oscillations over a wide range of parameter values. Many theoretical models have been proposed to explain the breakdown of steady flow, and somewhat fewer to describe the subsequent large amplitude oscillations. However, research in the area is still at the stage of discovering new potential mechanisms of breakdown, so the full description of the nonlinear oscillations that occur in a given experiment is a distant goal. It is the purpose of this paper to propose and explore yet another new mechanism of breakdown.

Previous theories of breakdown fall into two categories: models for which it can be shown that no steady flow exists for the parameter values of interest, and those for which a steady flow exists but is unstable. The familiar example of nonexistence is *choking*: one-dimensional, inviscid, steady flow in a uniform tube whose elastic properties are described by a tube law (a one-to-one relation between cross-sectional area and transmural pressure) cannot exist if the fluid speed is predicted to reach the propagation speed of small-amplitude long waves anywhere [17]. There is therefore a maximum flow rate above which no steady solution exists, for given values of P_e and P_d. The inclusion of longitudinal tension in the model

Contributed by the Bioengineering Division for publication in the JOURNAL OF BIOMECHANICAL ENGINEERING. Manuscript received by the Engineering Division October 25, 1990; revised manuscript received April 6, 1991.

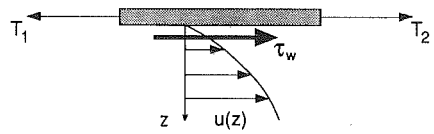

Fig. 1 The forces on an element of tube wall when fluid is flowing past with velocity $u(z)$ that increases with distance z from the wall. Because of the viscous shear force τ_w the downstream longitudinal tension T_2 is less than the upstream tension T_1.

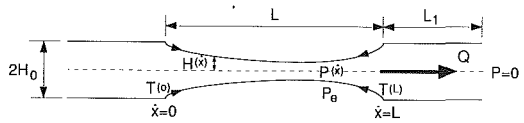

Fig. 2 Sketch of the model problem

does not alter this prediction, although the magnitude of the maximum flow rate increases with the tension [10]. However, the inclusion of energy loss, associated with flow separation at the narrowest part of a collapsed tube held open at its ends, appears to abolish such flow limitation and permits a steady solution to the model equations for all values of Q [10]. Instability theories include a variety of lumped-parameter models [1, 5, 12], flutter analyses [8], local instability of the "roll-wave" type [14], and global instability of the whole system, in which one-dimensional wave-propagation in the elastic tube is included, coupled to lumped models of the up and downstream parts of the system [4, 9].

The breakdown mechanism to be discussed in this paper comes into the former category, of nonexistence of steady flow, and can be outlined very simply. When viscous fluid flows in a tube it exerts a longitudinal shear stress on the wall. For elements of the wall to remain in equilibrium, therefore, the longitudinal tension $T(\hat{x})$ must decrease with distance $\hat{x}$ downstream (Fig. 1). For a given value of $T(0)$ at the upstream end of the tube $\hat{x} = 0$, and for a given flow rate Q, T may be expected to fall to zero somewhere if the tube is long enough. Alternatively, for a given length L of the tube and given $T(0)$, the wall shear τ_w will tend to increase with Q (this follows because $\tau_w \propto \bar{u}A^{-k}$ for some $k > 0$, where $\bar{u}$ is the average velocity, A tends to decrease as Q is increased as a result of the increased pressure drop, and $Q = \bar{u}A$); thus we would expect a maximum value of Q above which T is predicted to fall to zero for $\hat{x} < L$. If the wall tension became zero, the wall would be extremely flexible and may readily flutter; thus the prediction of zero longitudinal tension is assumed to correspond to the breakdown of steady flow. (Another physiological example where steady flow breakdown arises by the same mechanism occurs in a model of the flow of tightly fitting red cells in capillaries [16].) The present mechanism is somewhat different from that discussed briefly by Gottschalk and Sharp [6], who investigated the onset of buckling—i.e., collapse—of a circular tube when the circumferential tension fell to zero. Longitudinal viscous shear had an effect here too, via the Poisson's ratio of the wall material.

In this paper the reduction of longitudinal tension due to viscous shear is isolated from other effects and investigated in the simplest possible model. The flow conduit is taken to be a symmetric two-dimensional channel consisting of two rigid segments joined by a segment of length L of which the walls consist of thin membranes under tension (Fig. 2). Viscous incompressible fluid flows along the channel under the action of a pressure difference; the external pressure can be adjusted relative to the pressure at the downstream end of the system. The channel width is taken to be slowly varying, and the flow Reynolds number to be relatively small, so that lubrication theory can be used to describe the fluid motion. This approximation is not self-consistent when the downstream tension becomes small, because the wall slope becomes large then, but the results are expected to be of qualitative value.

An outline of the paper is as follows. The model is formulated quantitatively in the next section, in which the various dimensionless parameters governing the system are discussed. In Section 3, results are given for examples in which the axial tension T does not fall to zero at $x = L$, beginning with the relatively simple case of large axial tension, in which T varies by only a small fraction over the length of the channel. In Section 4 the case of greatest interest (but least accuracy in the model), in which the tension falls to zero at the downstream end of the channel, is considered, leading to the prediction of maximum flow rates for given values of $T(0)$ and L. In Section 5 the relation of $T(0)$ to the initial longitudinal tension or stretch before the flow is started is examined because of its importance experimentally. Further discussion is given in Section 6.

2 Formulation

The width of the rigid parts of the channel is taken to be $2H_0$; the upstream segment is arbitrarily long, while the downstream segment has length L_1 (Fig. 2). The slowly varying collapsible segment has width $2H(\hat{x})$ and length L (*so* $0 \le \hat{x} \le L$ in this segment). Lubrication theory is used to describe the fluid dynamics, so the pressure gradient is everywhere related to the flow-rate Q (per unit width of the channel) as it would be if the channel walls were parallel (Poiseuille's law):

$$P_{\hat{x}} = -\frac{3\mu Q}{2H^3} \text{ for } 0 \le \hat{x} \le L, \tag{2.1}$$

where P is the pressure in the fluid, $P_{\hat{x}}$ means $dP/d\hat{x}$, and μ is the viscosity of the fluid. The pressure drop along the downstream rigid segment is given correspondingly by

$$P(L) = \frac{3\mu Q L_1}{2H_0^3}, \tag{2.2}$$

where the pressure at the downstream end of the system (P_d) has been taken arbitrarily to be zero. Note that the validity of lubrication theory requires that the wall slope $H_{\hat{x}}$ should be small (and higher derivatives correspondingly smaller); in particular it is necessary that

$$\lambda = L/H_o \gg 1, \tag{2.3}$$

because even when the wall slope is everywhere small, it has a discontinuity at the ends (Fig. 2) so there will always be a small region at each end where the approximation is dubious. The Reynolds number $\rho Q/\mu$, where ρ is the fluid density, should be small enough that its product with the wall slope is also much less than 1.

There are two components of the force balance equation for an element of the membrane. The normal component states that the transmural pressure difference is equal to the tension $T(\hat{x})$ (per unit length in the perpendicular direction) multiplied by the curvature; in the slowly varying approximation this reduces to

$$P_e - P = TH_{\hat{x}\hat{x}}, \tag{2.4}$$

where P_e is the external pressure. The tangential component involves the shear stress and gives

$$T_{\hat{x}} = HP_{\hat{x}}; \tag{2.5}$$

this is the same as μ times the velocity gradient at the wall, equal to $HP_{\hat{x}}/\mu$ in Poiseuille flow. Equations (2.1), (2.4), and (2.5) are the nonlinear, ordinary differential equations governing the fourth-order system. The four boundary conditions are (2.2) together with

$$H(0) = H(L) = H_0 \tag{2.6}$$

and

$$\text{either } T(0) \text{ or } T(L) \text{ is assumed given.} \tag{2.7}$$

(It turns out to be more convenient mathematically and computationally to regard the downstream value of tension as given and the upstream one as to be found see the following.)

If we use the dimensions H_0 and L to scale the variables H and $\hat{x}$ in Eqs. (2.4) and (2.5), we find from the former that the pressure gradient has order of magnitude T_0H_0/L^3, where T_0 is a scale for the longitudinal tension, while the latter gives $\frac{1}{H_0}$ multiplied by the gradient in longitudinal tension, T'_o say. Thus

$$T_0' \sim \lambda^{-2} T_0/L,$$

from which we deduce that the change in T along the collapsible segment is $0(\lambda^{-2})$ times the absolute value of T. It follows that, under the lubrication approximation, the model is self-consistent only if the change in T is a small fraction of T. Equivalently, in examining cases in which the change in T is comparable with T, it is not self-consistent to use lubrication theory. Thus the results to be obtained will give an accurate solution of the model problem in the large tension limit (Section 3.1) but will give only a rough indication of the true mechanics in the case of greatest interest, when the downstream tension is very small, (Section 4). Indeed, we shall see that when the downstream tension tends to zero, the wall slope tends to infinity.

For mathematical purposes, the problem is most conveniently nondimensionalized as follows:

$$x=\hat{x}/H_0,\ y=H/H_0,\ t=\frac{2H_0T}{3\mu Q},\ t_0=\frac{2H_0T(0)}{3\mu Q},$$

$$t_\lambda=\frac{2H_0T(L)}{3\mu Q},\ p_o=\frac{2H_0^2[P_e-P(L)]}{3\mu Q}. \quad (2.8)$$

The pressure P can be eliminated by substituting (2.4) into (2.1) and (2.5), and we end up with two equations for $y(x)$ and $t(x)$:

$$t_x=-1/y^2 \quad (2.9)$$

$$(ty_{xx})_x=1/y^3, \quad (2.10)$$

subject to the boundary conditions

$$y(0)=y(\lambda)=1,\ t(0)=t_0 \text{ or } t(\lambda)=t_\lambda, \quad (2.11)$$

and

$$ty_{xx}|_{x=\lambda}=p_0. \quad (2.12)$$

Thus the three dimensionless parameters of the problem are the dimensionless length, λ (Eq. (2.3)), t_λ (or t_0) and p_0.

It is interesting to note that the only pressure difference that comes directly into the problem is $P_e - P(L)$, the transmural pressure at the downstream end of the collapsible segment. The same was found in the high-Reynolds-number, constant T, model of Jensen and Pedley [10], and confirms the proposal of Brower and Scholten [3] and Bertram et al. [2] that experimental results should be plotted in terms of this pressure difference, even if it is rather difficult to control experimentally.

The numerical problem represented by Eqs. (2.9)–(2.12), although involving only ordinary differential equations, is not very straightforward. In an experiment one would work with a tube of given length, mounted with a given degree of prestretch (related, but not equivalent, to a given value of $T(0)$—see Section 5); then for fixed values of $(P_e - P(L))$ one would vary Q and find the corresponding value of $T(L)$, if a solution exists. The most interesting result would be the critical value of Q for which $T(L)$ becomes zero. Numerically that would be equivalent to fixing λ, p_0, and t_0 and computing the value of t_λ; the relation between p_0 and t_0 when $t_\lambda = 0$ would be of particular interest. However, that problem is a fourth-order, two-point boundary value problem, with two boundary conditions at each end. It is much simpler to convert it first to a problem with three conditions at one end and one at the other, by regarding t_λ as given and t_0 as unknown, and then to treat λ as an unknown quantity so that each integration of the equations for which $y(x) - 1$ has more than one zero yields a solution of the problem for some values of the parameters.

We therefore transform the x-coordinate to

$$\xi=\lambda-x \quad (2.13)$$

and rewrite the governing equations as four first-order o.d.e.'s in terms of the four dependent variables t, y, $v = y'$, $w = tv'$, where a prime means $d/d\xi$, as follows:

$$t'=1/y^2,\ y'=v,\ v'=w/t,\ w'=-1/y^3. \quad (2.14)$$

The boundary conditions at $\xi = 0$ ($x = \lambda$) are taken to be

$$t(0)=t_\lambda,\ y(0)=1,\ v(0)=\beta,\ w(0)=p_0, \quad (2.15)$$

where β is the only constant not supposed given. A solution to the *physical* problem exists if the solution to the *mathematical* problem (2.14) and (2.15) involves $y(\xi)$ crossing the line $y = 1$ at some positive value of ξ. That is then the value of λ corresponding to the given values of t_λ, p_0, and β, while the value of t at $\xi = \lambda$ is t_0. As β is varied, other values of λ and t_0 corresponding to the same values of t_λ and p_0 may be found.

The solution to this problem for nonzero values of t_λ is given and discussed in the next section. The most interesting case, in which $t_\lambda = 0$, is not quite so simple because of the singularity that arises at $\xi = 0$ from the third of Eqs. (2.14). That case is dealt with in Section 4.

3 Nonzero Tension Everywhere

3.1 The Large Tension Limit. We begin with the limit of large t_λ for which, although the tension increases as ξ increases, the change is only a small fraction of t_λ. We could therefore postulate a simple expansion in powers of $1/t_\lambda$, but that turns out to be valid only for 0(1) values of λ and self-consistency of the lubrication approximation requires $\lambda \gg 1$. We therefore propose the following further rescaling of the problem

$$\bar{\xi}=t_\lambda^{-1/3}\xi,\ \bar{t}=t_\lambda^{-1}t,\ \bar{v}=t_\lambda^{1/3}v,\ \bar{w}=t_\lambda^{-1/3}w$$

under which the Eqs. (2.14) and boundary conditions (2.15) become as follows (where a prime now means $d/d\bar{\xi}$):

$$\bar{t}'=t_\lambda^{-2/3}/y^2,\ y'=\bar{v},\ \bar{v}'=\bar{w}/\bar{t},\ \bar{w}'=-1/y^3 \quad (3.1)$$

with

$$\bar{t}(0)=1,\ y(0)=1,\ \bar{v}(0)=\bar{\beta},\ \bar{w}(0)=\bar{p}_0 \quad (3.2)$$

where

$$\bar{\beta}=t_\lambda^{1/3}\beta,\ \bar{p}_0=t_\lambda^{-1/3}p_0. \quad (3.3)$$

If we suppose that $\bar{\beta}$ and $\bar{p}_0$ are 0(1) as $t_\lambda \to \infty$, we can postulate a series expansion in inverse powers of $t_\lambda^{2/3}$ of which the leading terms are

$$\bar{t}=1+t_\lambda^{-2/3}\bar{t}_1(\bar{\xi})+0(t_\lambda^{-4/3}),\ y=\bar{y}(\bar{\xi})+0(t_\lambda^{-2/3})$$

where

$$\bar{y}'''=-1/\bar{y}^3,\ \bar{t}_1'=1/\bar{y}^2 \quad (3.4a,b)$$

subject to

$$\bar{y}(0)=1,\ \bar{y}'(0)=\bar{\beta},\ \bar{y}''(0)=\bar{p}_0,\ \bar{t}_1(0)=0. \quad (3.5a,b,c,d)$$

Thus the problem is reduced to a third order one for $\bar{y}$, followed by a simple integral of (3.4*b*) for the first correction to $\bar{t}$. If, for a solution of (3.4*a*) and (3.5*a–c*), there is a positive value of $\bar{\xi}$, say $\bar{\lambda}$, such that $\bar{y}(\bar{\lambda}) = 1$, then the posed problem has a solution and the corresponding value of λ is given by

$$\lambda=t_\lambda^{1/3}\bar{\lambda}. \quad (3.6)$$

The corresponding estimate for t_0 is

$$t_0=t_\lambda[1+t_\lambda^{-2/3}\bar{t}_1(\bar{\lambda})]. \quad (3.7)$$

It is not mathematically obvious that even the restricted third-

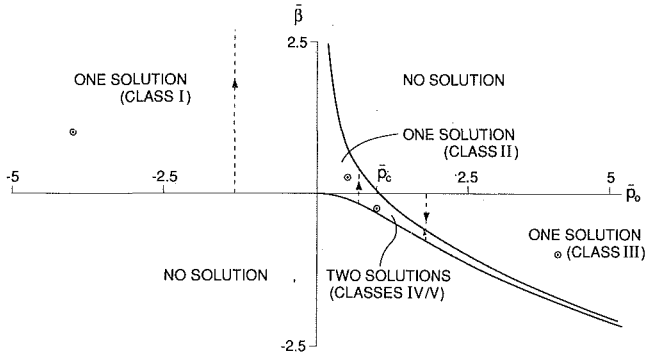

Fig. 3 The $\bar{p}_0 - \bar{\beta}$ plane, showing the regions in which there exist solutions of different classes to the problem defined by (3.4) and (3.5). The arrowed broken lines are paths along which $\bar{\lambda}$ increases from zero to infinity. The open circles correspond to the parameter values used in the calculation of Fig. 4.

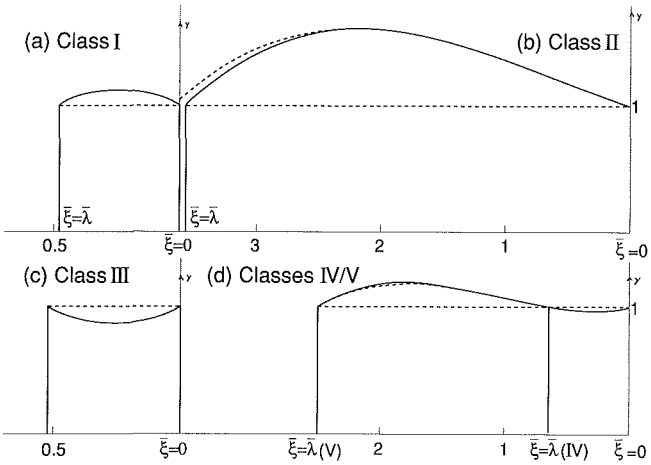

Fig. 4 Solid curves: graphs of $y(\bar{\xi})$ computed from (3.4) and (3.5) (large t_λ) for each of the five classes of solution; parameter values are as given in Table 1. In (*d*), the Class IV solution ends at the first zero of $y - 1$, Class V at the second. Dashed curves: the same plots computed from (3.1) and (3.2) with $t_\lambda = 64$ and the same values of $\bar{p}_0$ and $\bar{\beta}$ (distinguishable only in (*b*) and (*d*)). Note that $\bar{\xi} = 0$ represents the downstream end of the tube and has been placed at the right so that flow is from left to right.

order problem has a solution for all real values of $\bar{p}_o$ and for all positive values of $\bar{\lambda}$ (i.e., whether the original lubrication problem with uniform wall tension has a solution for all tube lengths and values of p_0), although on physical grounds one would expect it to do so. The conclusion can in fact be shown to be true; the proof will be given elsewhere.

Equations (3.4) have been solved numerically using a standard Runge-Kutta method [15]; the same method was used for all ordinary differential equations arising in this paper. Three-figure accuracy was checked by varying the internal and initial step-lengths, and by reintegrating the equations using different independent variables (see Section 4)). In terms of $\bar{p}_0$ and $\bar{\beta}$ the results can be listed, and the solutions categorized in four classes, as follows (see Fig. 3):

$\bar{p}_0 < 0$, $\bar{\beta} < 0$: there is no solution;
$\bar{p}_0 < 0$, $\bar{\beta} > 0$: there is always one solution (Class I);
$\bar{p}_0 > 0$, $\bar{\beta} \geq 0$: there is no solution unless $\bar{p}_0$ is less than a critical value which depends on $\bar{\beta}$, when there is one solution (Class II);
$\bar{p}_0 > 0$, $\bar{\beta} < 0$: there is either no solution, one solution (Class III), or two solutions (Classes IV and V), depending on the values of $\bar{p}_0$ and $\bar{\beta}$.

In the solutions of Class I, for a fixed negative value of $\bar{p}_0$ the value of $\bar{\lambda}$ increases from 0 to ∞ as $\bar{\beta}$ increases from zero to ∞. For fixed positive $\bar{p}_0$, $\bar{\lambda}$ increases from zero to infinity as $\bar{\beta}$ follows one of the arrowed paths through zones II and IV/V or III and IV/V: $\bar{\beta}$ decreases from zero along a branch where one solution exists until that disappears, and then increases again on the branch where two solutions exist (zone IV/V). The path ends on the upper bound of zone IV/V, for $\bar{p}_0 > \bar{p}_c$ (see Fig. 3) or the upper bound of zone II, for $\bar{p}_0 < \bar{p}_c$.

Table 1 Parameter values and results for examples of the five classes of solution to the problem for large tension, defined by (3.4) and (3.5)

Class	$\bar{p}_0$	$\bar{\beta}$	$\bar{\lambda}$	$\bar{t}_1$
I	−4.0	1.0	0.4841	0.4151
II	0.5	0.25	3.5520	1.9833
III	4.0	−1.0	0.5302	0.6372
IV	1.0	−0.25	0.6512	0.6823
V	1.0	−0.25	2.4975	2.1799

Examples of all five classes of solution are shown as graphs of $\bar{y}(\bar{\xi})$ in Fig. 4; the corresponding parameter values, including the value of $\bar{t}_1(\bar{\lambda})$ enabling t_0 be calculated from (3.7), are listed in Table 1 and the corresponding points marked on Fig. 3. We may note briefly that for solutions of classes I and II the channel is distended everywhere, while for those of classes III and IV it is (to some extent) collapsed everywhere. For solutions of class V it is distended in the upstream part and collapsed at the downstream end; such profiles of cross-sectional area are familiar both from experiments [5] and from other theoretical models (e.g., [10]).

3.2 Finite Tension. Analytical and numerical investigation of the full Eqs. (3.1) with boundary conditions (3.2) indicates that for each positive value of t_λ solutions exist that are qualitatively similar to those of (3.4) and (3.5). In particular the $\bar{p}_0 - \bar{\beta}$ plane is divided into regions in a similar way to Fig. 3, with the same number of solutions existing in each region and having the same general shape as depicted in Fig. 4. For example, if we take $t_\lambda = 64$, so $t_\lambda^{1/3} = 4$, then the values of $\bar{p}_0$ and $\bar{\beta}$ that led to the five solutions of Fig. 4 and Table 1 lead to almost indistinguishable solutions, as can be seen in Fig. 4. For each of the five cases, the values of $\bar{\lambda}$, λ, and t_0 are given in Table 2, together with the value of t_0 obtained from the large-t_λ asymptotic solution (Eq. (3.7) and Table 1). They are very close. For values of t_λ as low as 1.0, the same values of $\bar{p}_0$ and $\bar{\beta}$ can be used to generate solutions in each of the five classes; the values of λ and t_0 are also given in Table 2. Of course the corresponding tube length λ, from Eqs. (3.6), falls as t_λ falls, and in this particular example only the solutions in Classes III and V have λ sufficiently large compared with 1 (5.11 and 2.30, respectively) for the lubrication approximation to be reasonable. For $t_\lambda = 0.1$, the same values of $\bar{p}_0$ and $\bar{\beta}$ do not lead to a solution at all in Classes IV/V.

It is desirable to see what effect a reduction in longitudinal tension, as measured by t_λ, has on the shape of the channel walls for fixed values of p_0 and λ. Since collapsed channels, with positive p_0, are of greatest interest, we look in particular at the solutions of Classes IV and V, depicted in Fig. 4(*d*). The calculations for the dashed curves in that figure used $\bar{p}_0 = 1.0$ and had $\bar{\lambda} = 0.6627$ for Class IV, $\bar{\lambda} = 2.5042$ for Class V. When $t_\lambda = 64.0$, these values correspond to $p_0 = 4.0$ and $\lambda = 2.651$ and 10.017, respectively. We now show the channel shapes for the same values of p_0 and λ but for $t_\lambda = 0.1$; in the computations this means taking $\bar{p}_0 = 8.618$ and varying $\bar{\beta}$ until solutions are achieved with $\bar{\lambda} = 5.711$ and 21.581, respectively.

The results for channel half-width y are plotted against ξ (not $\bar{\xi}$) in Fig. 5; the two curves are for $t_\lambda = 64.0$ and 0.1. It can be seen that the lowering of tension results in much larger variations in channel width y, since hydrodynamic pressure

Table 2 **Parameter values and results for examples of the five classes of solution to Eqs. (3.1) and (3.2), for three values of t_λ (64.0, 1.0, and 0.1) and the same values of $\bar{p}_0$ and $\bar{\beta}$ as in Table 1. In the final column, t_0 (pred) is the value of t_0 calculated from (3.7) using the value of $\bar{t}_1$ from the large tension solution (Table 1), for comparison with the directly computed value of t_0 in the previous column.**

Class	$\bar{p}_0$	$\bar{\beta}$	t_λ	p_0	$\bar{\lambda}$	λ	t_0	t_0 (pred)
I	−4.0	1.0	64.0	−16.0	0.4883	1.953	65.67	65.66
			1.0	−4.0	0.5555	0.5555	1.471	1.415
			0.1	−1.857	0.9003	0.4179	0.4369	0.2927
II	0.5	0.25	64.0	2.0	3.656	14.623	72.11	71.93
			1.0	0.5	5.110	5.110	3.582	2.983
			0.1	0.2321	10.027	4.654	1.944	1.021
III	4.0	−1.0	64.0	16.0	0.5375	2.150	66.59	66.55
			1.0	4.0	0.6631	0.6631	1.814	1.637
			0.1	1.857	2.073	0.9620	1.451	0.396
IV	1.0	−0.25	64.0	4.0	0.6627	2.651	66.78	66.73
			1.0	1.0	0.8950	0.8950	1.942	1.682
			0.1	0.4641		NO SOLUTION		
V	1.0	−0.25	64.0	4.0	2.504	10.017	72.82	72.72
			1.0	1.0	2.298	2.298	3.249	3.180
			0.1	0.4641		NO SOLUTION		

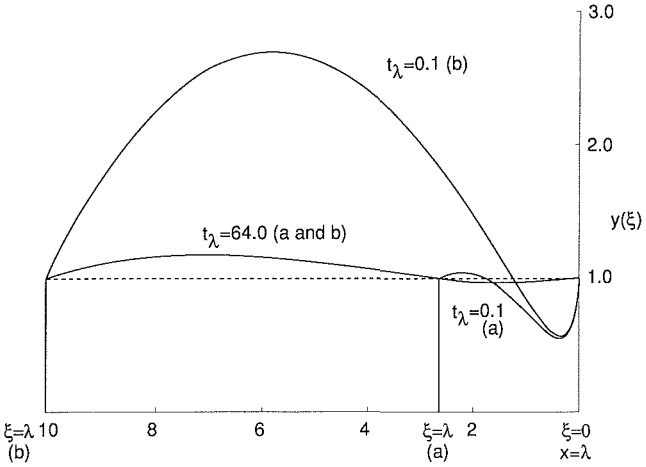

Fig. 5 **Graphs of $y(\xi)$ for $p_0 = 4.0$, $t_\lambda = 64.0$ and 0.1, and (*a*) $\lambda = 2.651$, (*b*) $\lambda = 10.017$. Note that $\xi = 0$ represents the downstream end of the tube, $x = \lambda$, and is on the right.**

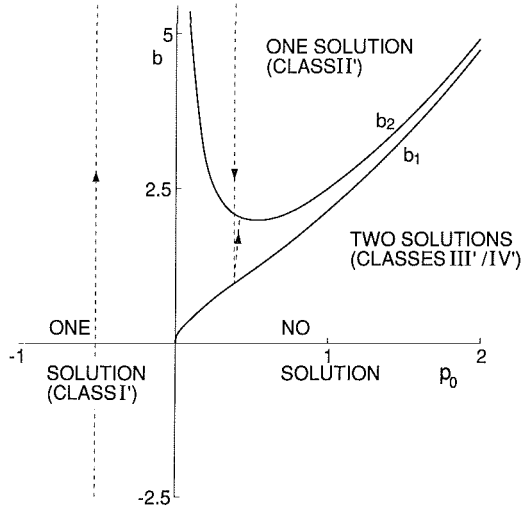

Fig. 6 **The $p_0 - b$ plane, showing the regions in which there exist solutions of different classes to the problem defined by (4.1) and (4.3). The arrowed broken lines are paths along which λ increases from zero to infinity.**

changes become relatively much more important. It is also apparent that the wall-slope does not remain small, especially at the downstream end of the collapsible segment, confirming that the model is not self-consistent in this case. Nevertheless, the qualitative features of the flow will be seen in practice: a sharp collapse, with steep slope, at the downstream end, and a distension upstream. For a given p_0, an increase in λ is accompanied by an increase in the extent of the distended region, and in the degree of distension. It does not result in a huge increase in upstream tension t_0 (t_0 = 45.3 and 51.7, respectively, in the shorter and longer examples of Fig. 5), because a large channel width (H) corresponds to a small wall shear, in proportion to H^{-2}, from (2.5) and (2.1).

4 Zero Tension at the Downstream End

In this case $t_\lambda = 0$, the Eqs. (2.14) are singular at $\xi = 0$ and we cannot use the rescaling of Section 3. However, the system can be reduced to third order, and arranged so that numerical integration is straightforward with no difficulties over accuracy, by transforming the equations so that t instead of ξ is the independent variable. The Eqs. (2.14) then become

$$\dot{y} = vy^2,\ \dot{v} = wy^2/t,\ \dot{w} = -1/y,\ \dot{\xi} = y^2, \qquad (4.1)$$

where a dot represents differentiation with respect to t, the dimensionless tension. The initial conditions on y, w, and ξ, from (2.15), are

$$y(0) = 1,\ w(0) = p_0,\ \xi(0) = 0; \qquad (4.2)$$

the condition on v will be given below. It can be seen that the first three equations represent the essential nonlinear system, and the fourth merely requires a single integration for ξ after the others have been solved. The singularity at $t = 0$ ($\xi = 0$) means that an analytical solution is required for small values of t, so that the integration can begin with finite values of the variables. The most general small-t solution of (4.1) with (4.2) is as follows:

$$y = 1 + t(p_0 \log t + b - p_0) + t^2\left[-\frac{1}{2} + (p_0 \log t + b)^2 - p_0^2 \log t - bp_0 - \frac{3}{2}p_0^2\right] + o(t^2) \qquad (4.3a)$$

$$v = p_0 \log t + b + t[-1 + 2p_0(p_0 \log t + b - 2p_0)] + o(t) \qquad (4.3b)$$

$$w = p_0 - t + \frac{1}{2}t^2(p_0 \log t + b - \frac{3}{2}p_0) + o(t^2) \qquad (4.3c)$$

$$\xi = t + t^2(p_0 \log t + b - \frac{3}{2}p_0) + o(t^2). \qquad (4.3d)$$

As could be inferred from (4.1), the singularity in v is logarithmic and determined by the value of p_0. (This logarithmic term corresponds to infinite wall-slope at the downstream end, so as already discussed the model is not self-consistent here.) The 0(1) correction to the logarithmic term in v is the arbitrary constant b, which corresponds to the constant β appearing in

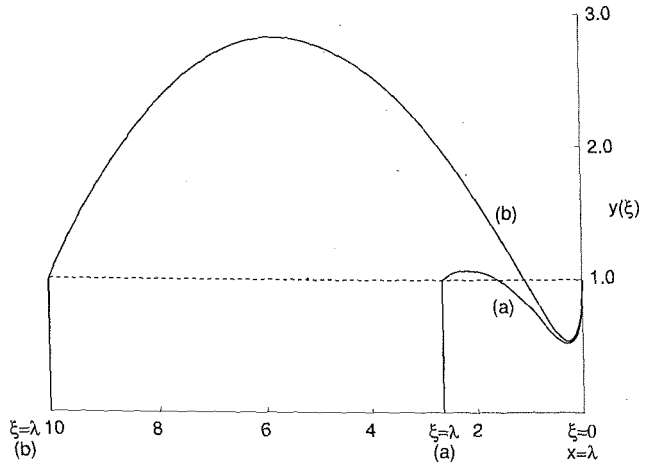

Fig. 7 Graphs of $y(\xi)$ for $t_\lambda = 0$, $p_0 = 4.0$ and (*a*) $\lambda = 2.651$, (*b*) $\lambda = 10.017$. Note that $\xi = 0$ is the downstream end of the tube, $x = \lambda$, and has been placed on the right.

(2.15). Starting from a small value of t (e.g., 0.001) at which the variables are evaluated using (4.3), integration of the equations proceeds in the positive t-direction until a value is reached at which $y - 1$ is again zero. That value of t is t_0, and the corresponding value of ξ is λ. For a given p_0, b can be varied to give different values of t_0 and λ.

The $p_o - b$ plane can be explored in the same way as the $\bar{p}_0 - \bar{\beta}$ plane was investigated in Section 3.1. Things are rather different in this case, because of the logarithmic term. For example, when $p_0 < 0$, $y - 1$ always starts out positive, because $\log t$ tends to $-\infty$ as t tends to zero, whereas the initial sign of $\bar{v}$ depended on the sign of $\bar{\beta}$. Similarly, when $p_0 > 0$, $y - 1$ starts out negative. We can see further, from (4.3*a*), that, if b has the same sign as p_0 and is much bigger than it, then $y - 1 = 0$ at a small value of t given by

$$t_0 \approx \exp[1 - b/p_0], \tag{4.4}$$

and a correspondingly small value of λ:

$$\lambda \approx t_0(1 - p_0 t_0/2). \tag{4.5}$$

Other mathematical details will be given elsewhere. Here we merely note that the $p_0 - b$ plane is divided into four regions, as shown in Fig. 6, and solutions to the problem exist or otherwise as indicated on that figure:

$p_0 < 0$: one solution exists for every value of b (Class I′)

$p_0 > 0$, $b < 0$: no solution exists

$p_0 > 0$, $b > 0$: there is no solution for $b < b_1$, one solution for $b > b_2$ (Class II′), and two solutions exist for $b_1 < b < b_2$ (Classes III′, IV′).

For fixed $p_0 < 0$, λ increases from zero to infinity as b increases from $-\infty$ to $+\infty$. For fixed $p_0 > 0$, λ increases from zero to infinity as b follows the arrowed path, decreasing from $+\infty$ to b_1 and then increasing (along the second solution branch) to b_2.

Solutions of Class I′, ($p_0 < 0$) represent channels which are distended everywhere, while for $p_0 > 0$ the channels are collapsed somewhere; for larger values of λ, however (Class IV′ solutions) the tube is distended over much of its length. Figure 7 includes the graphs of $y(\xi)$ for $p_0 = 4.0$ and $\lambda = 2.651$ and 10.017, for comparison with Fig. 5. The differences are not great.

The main results, however, are plots of t_0 versus λ for different values of p_0, since these give the critical values of upstream tension for given p_0 and λ. Such plots for $p_0 = -1$, -0.1, 0.1, 1.0 and 10.0 are given in Fig. 8. For negative p_0, there is only a limited range of values of λ ($0 < \lambda < \lambda_c$) for which a critical value of t_0 exists. When $\lambda > \lambda_c$, the downstream

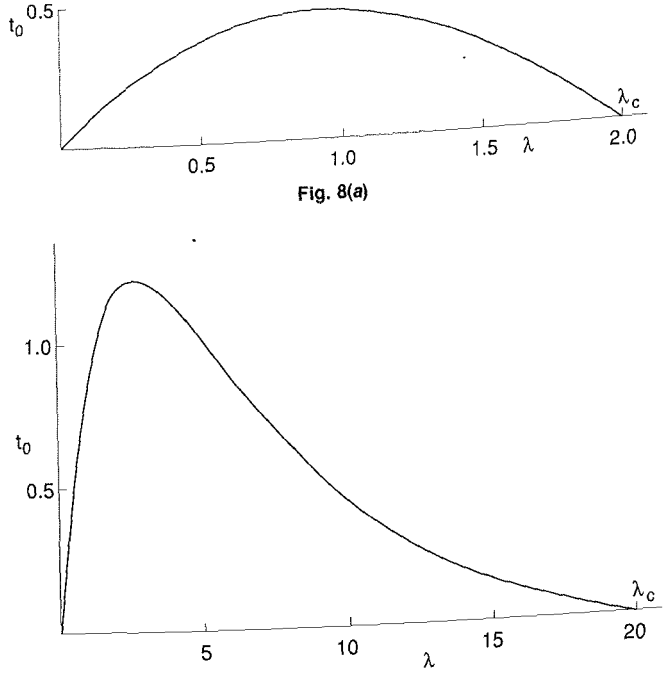

Fig. 8 Graphs of the critical value of upstream tension t_0, below which no solution exists with $t_\lambda = 0$, plotted against channel length λ, for different values of p_0. (*a*) $p_0 = -1.0$, (*b*) $p_0 = -0.1$, (*c*) $p_0 = +0.1$, $+1.0$, and $+10.0$.

tension t_λ must be positive for a steady flow to be possible; this is because the channel is very distended, and the wall shear is therefore very small, over most of its length. Such a case is physically unrealistic. For positive p_0 the channel is collapsed and the wall shear therefore high over some part of its length, so there is a critical value of t_0 for all lengths. This critical value does tend to zero as λ tends to infinity, but it does so extremely slowly even at the smallest chosen value of p_0, equal to 0.1.

5 The Relation to Initial Tension or Stretch

The critical values of dimensionless tension plotted in Fig. 8 are the values at the upstream end of the channel, given that the downstream tension is zero. For experimental purposes it would be desirable to relate these results to the uniform longitudinal tension or stretch present in the channel wall before the fluid starts to flow. Such a relationship can be derived if we recall that the slope of the channel wall must be very small for lubrication theory to be valid; the overall length of the membranes therefore remains approximately constant, with an error that is second order in wall slope. Individual elements of the wall, however, will change their length once flow begins, because of the change in longitudinal tension.

With reference to Fig. 9, suppose the membrane to be divided

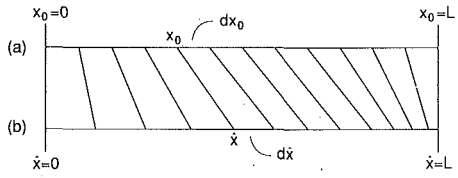

Fig. 9 Sketch indicating (*a*) the stretched membrane in the absence of flow, (*b*) the stretched membrane when the fluid is flowing; the element of length dx_0 at position x_0 changes length to $d\hat{x}$ and is shifted to position $\hat{x}$.

into elements of equal unstretched length dl, and let it be initially stretched by tension T_0 so that each such element has length dx_0. The initial stretch ratio, S_0, is then defined by

$$S_0 = \frac{dx_0}{dl} = \frac{L}{l}, \tag{5.1}$$

where l is the overall unstretched length and L is the stretched length. Suppose that, when the fluid flows, the element dx_0 at position x_0 changes its length to $d\hat{x}$ and its position to $\hat{x}$; the new stretch ratio is

$$S(\hat{x}) = d\hat{x}/dl. \tag{5.2}$$

Rewriting this expression as $dl = d\hat{x}/S(\hat{x})$, and integrating over the length of the membrane, we obtain

$$l = \int_0^L \frac{d\hat{x}}{S(\hat{x})}. \tag{5.3}$$

We further suppose that the membrane elasticity can be represented by a single-valued function relating the stretch ratio to the longitudinal tension $T(\hat{x})$:

$$S(\hat{x}) = F[T(\hat{x})]; \tag{5.4a}$$

in particular

$$S_0 = F(T_0). \tag{5.4b}$$

Thus we finally obtain

$$l = \int_0^L \frac{d\hat{x}}{F[T(\hat{x})]}, \tag{5.5}$$

which can be made dimensionless using the expressions (2.8) and provides a relationship between the solution of the fluid mechanical problem, in the form of $T(\hat{x})$, and the initial stretch ratio S_0 or tension T_0.

For a simple example we take the membrane to be linearly elastic, so that (5.4*a*) can be written

$$S - 1 = T/E, \tag{5.6}$$

where E is the modulus of elasticity, assumed constant. Then (5.5) becomes

$$l = \int_0^L \frac{1}{1 + T/E}\, d\hat{x}. \tag{5.7}$$

On nondimensionalization and transformation to the variable ξ (Eq. (2.13)) this can be written

$$\frac{l}{H_0} = \int_0^\lambda \frac{d\xi}{1 + \kappa t(\xi)}, \tag{5.8}$$

where

$$\kappa = \frac{3\mu Q}{2H_0 E}; \tag{5.9}$$

on further transforming to t as the independent variable, as in (4.1), we obtain

$$\frac{l}{H_0} = \frac{\lambda}{S_0} = \int_{t_\lambda}^{t_0} \frac{y^2 dt}{1 + \kappa t}. \tag{5.10}$$

Thus, given κ, the numerical results of earlier sections can be used to compute l/H_0, which can then be compared with λ to see the initial stretch corresponding to a particular solution. Note from (5.9) that, for a given value of E, κ is a measure of the flow rate. For the cases of $\lambda = 2.651$ and 10.017 with $p_0 = 4.0$, used above for various examples, the integral in (5.8) or (5.10) has been performed for various values of t_λ (= 0, 0.1, 64.0) and of κ (0.01, 0.1, 1.0). The results are given in the form of the initial stretch ratio S_0 in Table 3. We can see that when κt_λ is large the values of the stretch ratio are absurdly large; this is because $\kappa t = T/E$ is the same as the strain $S - 1$, so large κt_λ means large strain even at the downstream end of the channel, and hence even larger strain further upstream. Examples with a realistic initial strain of 25–35 percent include those with small or zero t_λ and $\kappa = 0.1$. The similarlity between the values obtained for $t_\lambda = 0$ and $t_\lambda = 0.1$ is not physically surprising, but represents a useful check on the calculations since the $t_\lambda = 0$ values were obtained by integrating (4.1) and (5.10) while for $t_\lambda \neq 0$, Eqs. (3.1) and (5.8) were used.

Table 3 The initial stretch S_0 corresponding to different values of t_λ and κ, for two values of the stretched channel length λ and for $p_0 = 4.0$

λ	t_λ	κ	S_0
10.017	64.0	0.01	1.69
		0.1	7.86
		1.0	69.6
	0.1	0.01	1.04
		0.1	1.36
		1.0	4.27
	0.0	0.01	1.04
		0.1	1.34
		1.0	4.12
2.651	64.0	0.01	1.65
		0.1	7.54
		1.0	66.3
	0.1	0.01	1.03
		0.1	1.27
		1.0	3.18
	0.0	0.01	1.03
		0.1	1.27
		1.0	3.18

6 Further Discussion

The two main questions to be answered by future work are (*a*) how should we make the model more self-consistent and realistic, and (*b*) what happens after breakdown, in conditions for which T is predicted to fall to zero at or before $\hat{x} = L$?

Self-consistency of the two-dimensional membrane model can be achieved by abandoning the lubrication approximation. First, the full expression for the curvature can be inserted into (2.4); that is easy. Second, the expression (2.1) must be abandoned in favor of a full numerical solution of the Navier-Stokes equations (or, at low Reynolds number, the Stokes equations). This is of course a much more difficult project, but it is within the scope of present-day computational fluid dynamics, and is currently being initiated. We do not anticipate significant qualitative changes to the results.

To go further, however, and incorporate the three-dimensional elasticity of a real flexible tube, even thin-walled, is significantly more difficult still, especially when coupled with three-dimensional fluid mechanics. This is yet to be undertaken.

What happens in the model problem after the longitudinal tension falls to zero? Here again we do not know. In most experiments oscillations occur for some parameter values, but whether these are associated with zero tension is unknown. Whether unsteady behavior can develop at low Reynolds numbers is also unknown, since most experiments have been at high Reynolds numbers. In some experiments with thin-walled tubes, part of the tube is sucked intermittently into the downstream rigid segment, which could not be described by anything

like the present model. Steep wall slope, as predicted here, is associated with flow separation even at low Reynolds numbers, and that predisposes the flow to becoming unstable [4, 13]. But what unsteady behavior, if any, is directly attributable to the tension falling to zero remains an open question.

Acknowledgments

The author is indebted to P. A. Stewart for an enlightening conversation. He is also grateful to Professor R. M. Nerem and the George W. Woodruff School of Mechanical Engineering, Georgia Institute of Technology, for their hospitality during the period when this work was begun.

References

1 Bertram, C. D., and Pedley, T. J., "A Mathematical Model of Unsteady Collapsible Tube Behaviour," *J. Biomech.*, Vol. 15, 1982, pp. 39–50.

2 Bertram, C. D., Raymond, C. J., and Pedley, T. J., "Mapping of Instabilities During Flow Through Collapsed Tubes of Differing Length," *J. Fluids & Structures*, Vol. 4, 1990, pp. 125–154.

3 Brower, R. W., and Scholten, C., "Experimental Evidence on the Mechanism for the Instability of Flow in Collapsible Vessels," *Med. & Biol. Engineering*, Vol. 13, 1975, pp. 839–845.

4 Cancelli, C., and Pedley, T. J., "A Separated Flow Model for Collapsible Tube Oscillations," *J. Fluid Mech.*, Vol. 157, 1985, pp. 375–404.

5 Conrad, W. A., "Pressure-Flow Relationships in Collapsible Tubes," *IEEE Trans. on Bio-med. Engineering*, Vol. BME-16, 1969, pp. 284–295.

6 Gottschalk, S., and Sharp, B. B., "The Banki Paradox," *Proc. 5th Canadian Congress of Applied Mechanics*, 1975, pp. 493–494.

7 Griffiths, D. J., "Oscillations in the Outflow From a Collapsible Tube," *Med. & Biol. Eng. & Comput.*, Vol. 15, 1977, pp. 357–362.

8 Grotberg, J. B., and Gavriely, N., "Flutter in Collapsible Tubes: A Theoretical Model of Wheezes," *J. Appl. Physiol.*, 1989, Vol. 66, pp. 2262–2273.

9 Jensen, O. E., "Instabilities of Flow in a Collapsed Tube," *J. Fluid. Mech.*, Vol. 220, 1990, pp. 623–659.

10 Jensen, O. E., and Pedley, T. J., "The Existence of Steady Flow in a Collapsed Tube," *J. Fluid Mech.*, Vol. 206, 1989, pp. 339–374.

11 Kamm, R. D., and Pedley, T. J., "Flow in Collapsible Tubes: A Brief Review," ASME JOURNAL OF BIOMECHANICAL ENGINEERING, Vol. 111, 1989, pp. 177–179.

12 Katz, A. I., Chen, Y., and Moreno, A. H., "Flow Through a Collapsible Tube," *Biophys. J.*, Vol. 9, 1969, pp. 1261–1279.

13 Matsuzaki, Y., and Fung, Y. C., "On Separation of a Divergent Flow at Moderate Reynolds Numbers," ASME *Journal Appl. Mech.*, Vol. 98, 1976, pp. 227–231.

14 Pedley, T. J., "The Fluid Mechanics of Large Blood Vessels," Cambridge University Press, Section 6.4, 1980.

15 Press, W. H., Flannery, B. P., Teukolsky, S. A., and Vetterling, W. T., *Numerical Recipes: The Art of Scientific Computing*, Cambridge University Press, 1986.

16 Secomb, T. W., and Skalak, R., "A Two-Dimensional Model for Capillary Flow of an Asymmetric Cell," *Microvascular Res.*, Vol. 24, 1982, pp. 194–203.

17 Shapiro, A. H., "Steady Flow in Collapsible Tubes," ASME JOURNAL OF BIOMECHANICAL ENGINEERING, Vol. 99, 1977, pp. 126–147.